processes

Article

Microbialite Textures and Their Geochemical Characteristics of Middle Triassic Dolomites, Sichuan Basin, China

Hao Wang [1,2,3], Ziquan Yong [1,*], Jinmin Song [1,*], Tong Lin [1] and Yongqiang Yu [1]

1 State Key Laboratory of Oil and Gas Reservoir Geology and Exploitation, Chengdu University of Technology, Chengdu 610059, China; wanghao2012cdut@163.com (H.W.)
2 Department of Geology, University of Regina, Regina, SK S4S 0A2, Canada
3 Shudao Investment Group Limited Liability Company, Chengdu 610031, China
* Correspondence: yongzq@cdut.edu.cn (Z.Y.); songjinmin2012@mail.cdut.edu.cn (J.S.)

Abstract: Microbialite textures, such as microbial mats and biofilms, were observed in the Middle Triassic dolomite in the Sichuan Basin, western China, using core examination, thin section petrography, scanning electron microscopy (SEM), and geochemical analyses. The dolomite texture, consisting of fibrous and spherulitic structures, is similar in morphology and size distribution to those observed in microbial culture experiments. Extracellular polymeric substances (EPS) were identified based on the occurrence of fibers forming a reticular pattern and nanometer-sized spheroids. The rare earth element (REE) and stable isotope (C, O, and Sr) compositions of the Middle Triassic dolomite were measured to determine their geochemical characteristics. Using seawater as a standard, the dolomitic microbialites (MD) exhibited significantly positive La and Eu anomalies and higher REE concentrations and $(Nd/Yb)_{sn}$ values than associated limestones, and these patterns are inferred to be related to initial complexation on organic ligands in the biofilm, as proposed by previous researchers. The ambient temperature during dolomite precipitation was estimated to be within the 23 °C to 50 °C range, as indicated by the $\delta^{18}O$ values of the dolomite. This study suggests that various microbial effects can significantly affect diagenetic processes in the Middle Triassic dolomite.

Keywords: Sichuan Basin; Leikoupo Formation; microbialites; dolomites; diagenesis

check for updates

Citation: Wang, H.; Yong, Z.; Song, J.; Lin, T.; Yu, Y. Microbialite Textures and Their Geochemical Characteristics of Middle Triassic Dolomites, Sichuan Basin, China. *Processes* **2023**, *11*, 1541. https://doi.org/10.3390/pr11051541

Academic Editors: Yinhui Zuo and Hui Han

Received: 17 April 2023
Revised: 11 May 2023
Accepted: 15 May 2023
Published: 17 May 2023

Copyright: © 2023 by the authors. Licensee MDPI, Basel, Switzerland. This article is an open access article distributed under the terms and conditions of the Creative Commons Attribution (CC BY) license (https://creativecommons.org/licenses/by/4.0/).

1. Introduction

The distribution and behavior of aqueous rare earth elements (REEs) are widely used to constrain the source of fluids and formation conditions of sedimentary rocks [1]. In recent years, researchers have employed the REE signatures and isotopic compositions (e.g., C, O, and Sr) of dolomites to examine the nature of dolomitization [2–4]. Laboratory experiments have also demonstrated the role of microbes in dolomite precipitation [5,6]. The REE and isotope signatures of microbialites have successfully been utilized to analyze seawater and lacustrine waters [7], the geochemistry of microbial mounds [8], the role of the organic substrate on microbially mediated dolomite [9], and the origin of microbialites [10,11]. Despite extensive research, the impact of the diagenetic environment and the evolution of fluid chemistry on dolomitization remains a topic of heated debate [12–15].

The Middle Triassic Leikoupo Formation is an assemblage of gypsum-dominated evaporites and carbonates that form the uppermost unit in the Sichuan carbonate platform succession [16]. In recent years, the Leikoupo Formation has gradually become the primary exploration target in the western and central Sichuan Basin [17], where high-quality reservoirs are exclusively restricted to dolomites [18,19]. The Leikoupo dolomite in the Sichuan Basin is interpreted to have formed in three stages: The penecontemporaneous stage characterized by evaporative seawater, the early diagenetic stage characterized by seepage refluxed brine, and the burial stage [20]. Previous papers primarily focused on crystalline dolomite and dolomitic grainstone. Liu [21] reports petrographic and reservoir characteristics on the microbial dolomite in the western Sichuan Basin, which has a cumulative thickness of 0 to 70 m locally and forms high-quality reservoirs.

This study aimed to characterize the REE and Sr-O-C isotope geochemical signature of the microbial dolomite in the Middle Triassic Leikoupo Formation in the Sichuan Basin. The results of the study could also lead to a better understanding of the morphogenesis of microbialites, their evolution through geologic time, and their potential as tools for biostratigraphic correlation.

2. Geological Setting

The study area is located in Pengzhou near Chengdu (southwestern China) on the western margin of the Sichuan Basin (Figure 1). The Sichuan Basin, surrounded by the Longmen, Micang, and Daba mountains, is a large intracratonic basin with an area of approximately 180,000 km^2 in the upper Yangtze region of South China. Since the Mesozoic, the basin has experienced deep fault activity on its margins and underlying crustal shortening, which has led to both peripheral subsidence and internal uplift. Moreover, the tectonic setting of the basin is such that the basin has been subjected to external pressure and internal extension. Marine sedimentation dominated the basin from the Precambrian to the Middle Triassic. At the end of the Middle Triassic, the Sichuan Basin was an epeiric sea subject to tides and waves and was connected to the open ocean in the southern and northwestern parts of the basin under the influence of the early Indosinian Orogeny. The climate during this period was arid and hot.

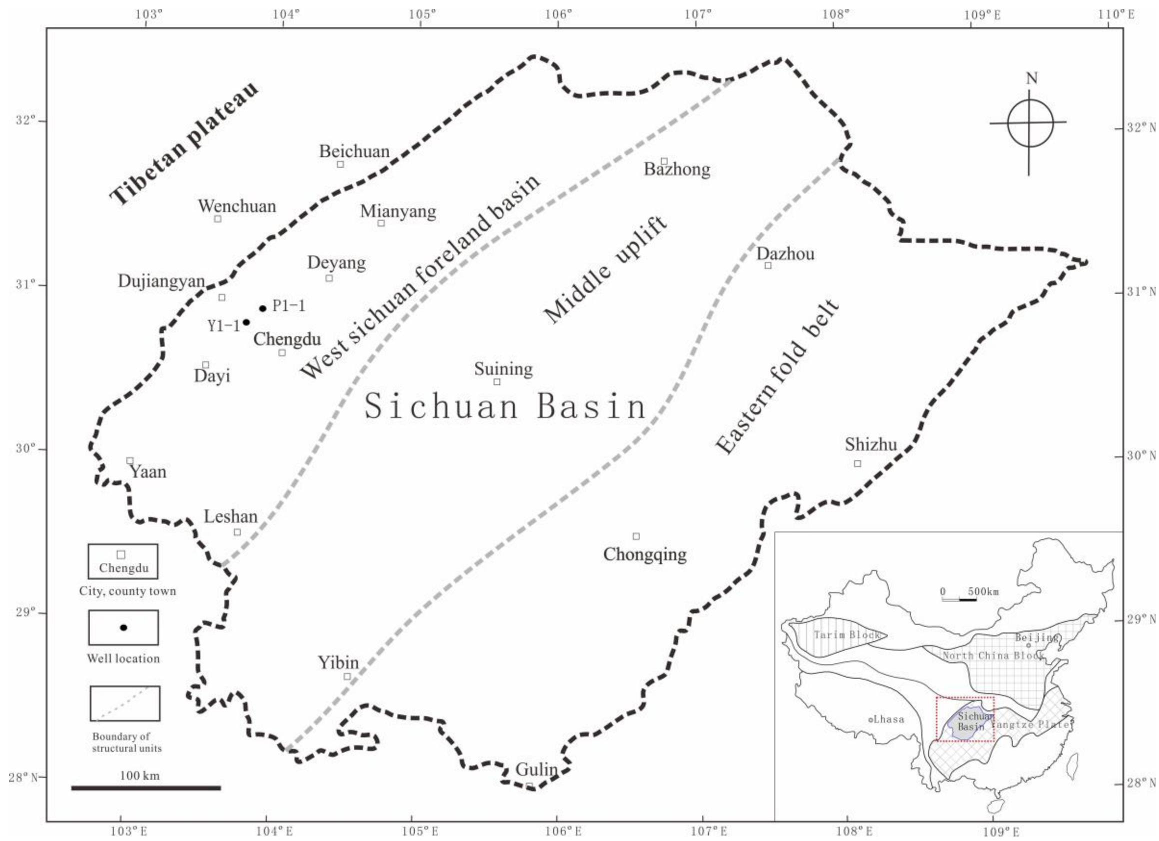

Figure 1. Location map of the study area in the Sichuan Basin, southwestern China.

The Leikoupo Formation (T_2l) is underlain by the Jialingjiang Formation and overlain by the Tianjingshan Formation, with both upper and lower contacts being conformable (Figure 2). The Leikoupo Formation is characterized by multiple cycles of marine carbonates and evaporites, including limestones, dolomites, gypsum, and salts with thicknesses varying from 0 to over 1100 m (Figure 2), along with local muddy deposits. The formation can be divided into four members, with the T_2l_1 being the lowermost member that conformably overlies the Jialingjiang Formation. The fourth member (T_2l_4) is the uppermost member that directly underlies the Tianjingshan Formation in the western zone (Figure 2). The fourth member (T_2l_4) can be further subdivided into three submembers, the Lei 4^1 submember, Lei 4^2 submember, and Lei 4^3 submember. In the western zone, Lei 4^1 consists of thick gypsum interbedded with dark micritic dolomites; Lei 4^2 consists of interbedded gypsum and micritic dolomites; and Lei 4^3 consists of micritic dolomites, fine crystalline dolomites, limy dolomites, algae trace dolomites, dolomitic limestones, and calcarenites (Figure 2). Our research focuses on the Lei 4^3 submember, which consists of algal/microbial dolomites, and is based on core observation, thin section analysis, and scanning electron microscope observations.

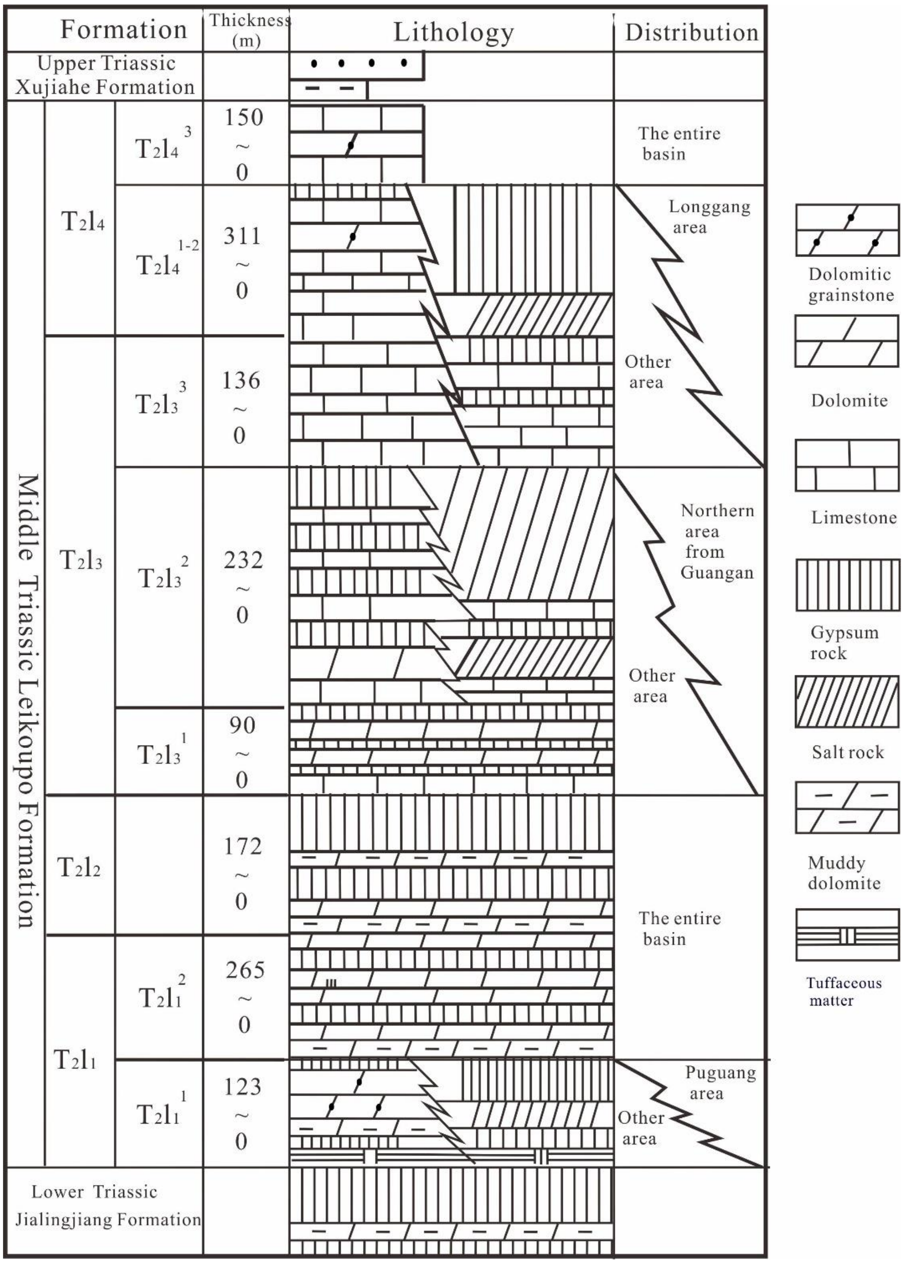

Figure 2. Generalized stratigraphy of the Leikoupo Formation, Sichuan Basin (modified after Li et al., [15]). T_2l_1, T_2l_2, T_2l_3, and T_2l_4 represent the first to fourth members of the Leikoupo Formation. Lei 4^1, Lei 4^2, and Lei 4^3 represent the first to third submembers of T_2l_4.

3. Samples and Analytical Methods

A total of 45 samples of the Lei 4^3 submember were collected from 2 cored wells (Figure 3). Some thin sections were stained with Alizarin Red to identify dolomite and calcite. The samples were investigated through stratigraphic and sedimentological methods, optical petrography (Figure 4), and scanning electron microscopy (SEM). To evaluate the micropore features, fresh samples with relatively flat tops and bottoms (with lengths, widths, and heights of <0.5 cm) were plated (100 s) with gold. A Nova Nano SEM 450 was used for scanning electron microscopy with an ultrahigh resolution (1.0 nm at 15 kV to 1.6 nm at 1 kV).

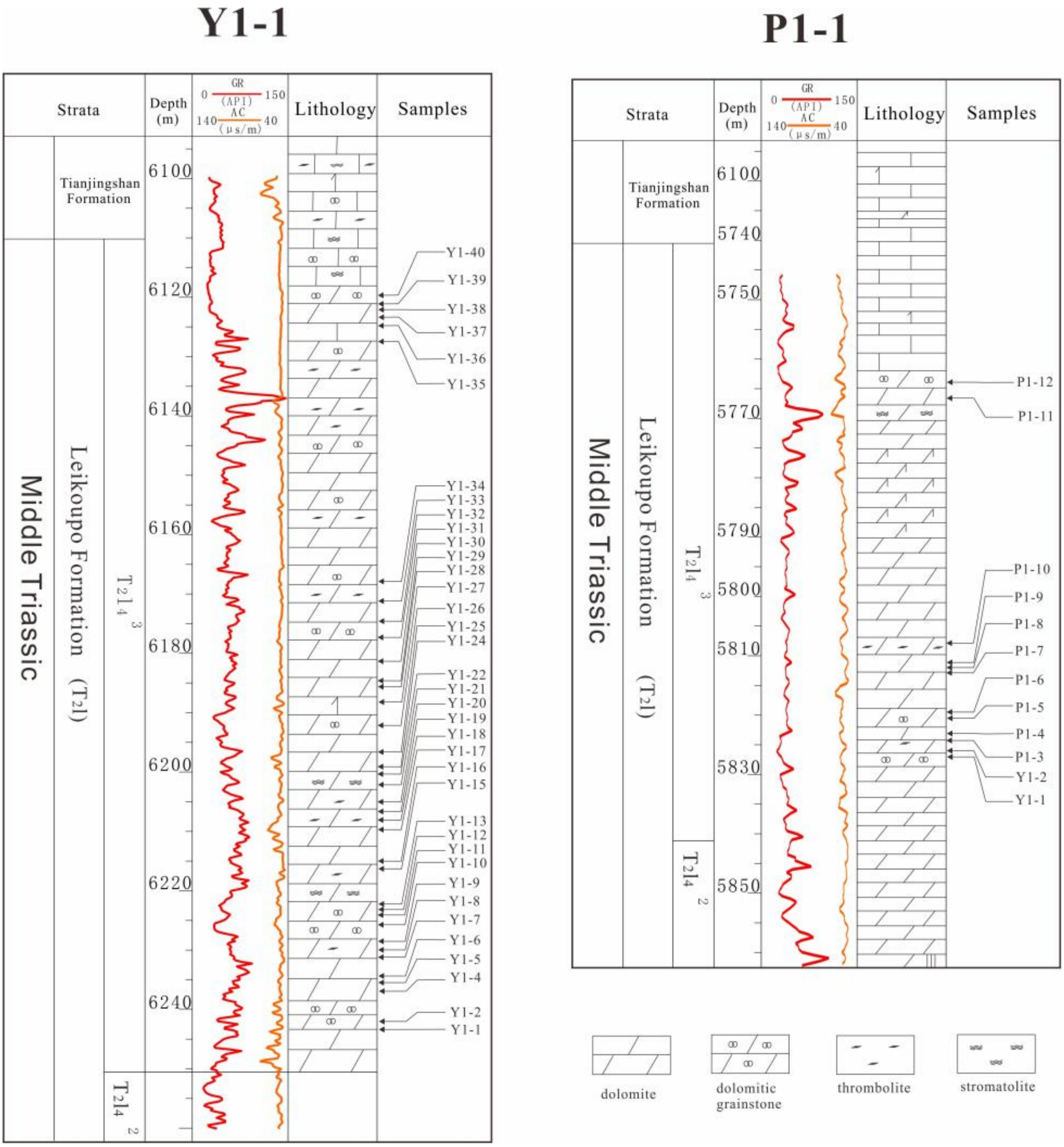

Figure 3. Lithofacies and well logs of the P1-1 and Y1-1 wells. Arrows represent the sampling sites. The lithology was characterized on the basis of drill cuttings and core observations. See Figure 1 for the location of wells. GR = gamma-ray logging; AC = acoustic logging.

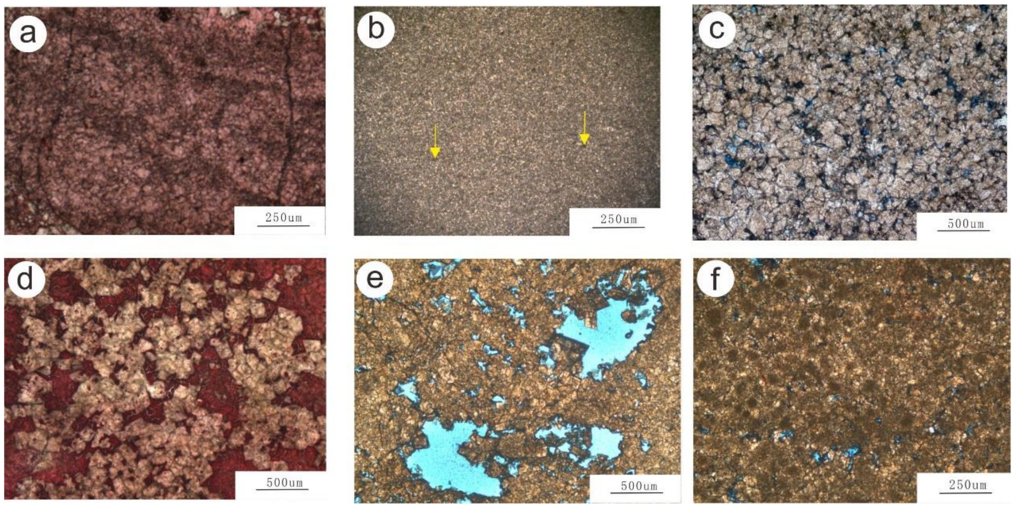

Figure 4. Petrographic features of the studied limestone, calcitic dolomite, and dolomite from the Leikoupo Formation. (**a**) Y1-36 is primarily composed of calcite with a crystal size of less than 30 µm. The thin sections were stained with Alizarin Red-S. (**b**) Photomicrograph of very finely to finely crystalline dolomites with crystal sizes of less than 30 µm. Pyrite (arrows) disseminated in intercrystalline pores. Y1-8, 6230.02 m. (**c**) Photomicrograph of finely to medium crystalline dolomites with irregular vugs; the size of the dolomite crystals varies between 45 mm and 150 µm. Y1-7, 6231.10 m. (**d**) Photomicrograph of finely to medium crystalline dolomites replacing precursor limestones (stained red with Alizarin Red-S). Y1-30, 6181.2 m. (**e**) Photomicrograph of the intergranular dissolved pores developed in the finely to medium crystalline dolomites; some crystals have cloudy centers and clear rims. Y1-31, 6177.22 m. (**f**) Photomicrograph of the pelletal dolomitic grainstone. Y1-13, 6222.71 m.

Isotope samples were analyzed at the Chengdu University of Technology. Carbon and oxygen isotope values were measured using a Thermo Electron mass spectrometer (MAT 252) and reported in per mil notation relative to the Vienna Pee Dee Belemnite (VPDB) standard. Carbonate powders were reacted with 100% phosphoric acid at 25 °C for 72 h. Stable isotope results were calibrated with carbonate standard GBW04417 calcite. The analytical precision is higher than 0.2‰ for both $\delta^{18}O$ and $\delta^{13}C$. Isotopic measurements of Sr were performed on a Triton Plus thermal ionization mass spectrometer (Thermo Fisher Scientific, Berlin, Germany). The results were controlled by repeated analyses of 2 international standard samples, NBS-987 and BCR-2.

Major element analysis of the rock samples was conducted at the Institute of Geology and Geophysics, Chinese Academy of Sciences (IGGCAS) using the melted glass disk method and X-ray fluorescence spectrometry. The chemical composition of the samples was analyzed using X-ray fluorescence (XRF) spectrometry on fused glass disks, following the analytical procedure outlined by Johnson [22]. The accuracy and precision of the XRF data from the laboratory were evaluated based on results obtained for USGS standard BCR-2 and Chinese National standard GSR-3. The analysis precision of this method is better than 5%. The major elements used for analysis were Al_2O_3, Fe_2O_3, MgO, and CaO.

The trace elements of the samples were analyzed using an inductively coupled plasma mass spectrometer (Thermo X-7, Thermo-Elemental Corp, San Jose, CA, USA). The analysis was performed with the standard curve method, with Rh, In, and Re as the internal standards, at an analysis precision of 5–10%. The exact process was described by Wu et al. [23]. The analyzed trace elements were Si, Ti, V, Cr, Co, Ni, Cu, Zn, Sr, Y, Zr, Mo, Cd, Sn, Sb, Ba, La, Ce, Pr, Nd, Sm, Eu, Gd, Tb, Dy, Ho, Er, Tm, Yb, Lu, Th, and U.

The quantitative elemental analytical results are listed in Table 1. The measured REE concentrations were normalized to the REE compositions in surface Pacific water. The REE composition of seawater was magnified 1,000,000 times because the ΣREE of dolomite is enriched by six orders of magnitude or higher with respect to seawater. The ratio $(Nd/Yb)_{sn}$

was calculated to monitor light REE (LREE) depletion. The ratio $(Dy/Yb)_{sn}$ was calculated to monitor heavy REE (HREE) depletion. We use the method reported by Bau [24] and Webb [25] to report Ce anomalies. Ce_{sn} anomalies are shown by $(Ce/Ce^*)_{sn}$, which is calculated as $Ce_{sn}/(0.5\ La_{sn} + 0.5\ Pr_{sn})$. Then, $(Pr/Pr^*)_{sn}$ $[Pr_{sn}/(0.5\ Ce_{sn} + 0.5\ Nd_{sn})]$ is calculated and compared to $(Ce/Ce^*)_{sn}$ $[Ce_{sn}/(0.5\ La_{sn} + 0.5\ Pr_{sn})]$. When $(Pr/Pr^*)_{sn} > 1$, a negative Ce_{sn} anomaly exists; when $(Pr/Pr^*)_{sn} < 1$, a positive Ce_{sn} anomaly exists. The combination of $(Ce/Ce^*)_{sn} < 1$ and $(Pr/Pr^*)_{sn} \approx 1$, however, indicates a positive La_{sn} anomaly.

Table 1. REE contents, stable and radioactive isotope compositions and trace element concentrations for carbonate samples in the western Sichuan Basin. All concentrations are in parts per million (ppm), except where noted. C and O isotope compositions are both reported relative to V-PDB. BT, the concentrations are below detection limits.

Sample NO.	Depth (m)	La	Ce	Pr	Nd	Sm	Eu	Gd	Tb	Dy	Ho	Er	Tm	Yb	Lu	ΣREE	Th	Zr	Ti	Ba	$\delta^{13}C$	$\delta^{18}O$	Sr	$^{87}Sr/^{86}Sr$
Very finely to finely dolomites																								
P1-3	5824.25	0.233	0.452	0.055	0.219	0.039	0.009	0.043	0.007	0.035	0.008	0.019	0.003	0.018	0.003	1.143	0.07	1.507	36.57	11.33	1.63	−3.26		
Y1-12	6199.20	0.263	0.414	0.049	0.175	0.031	0.007	0.026	0.006	0.03	0.005	0.016	0.002	0.014	0.003	1.041	0.08	0.617	22.31	2.4	2.32	−4.09	155.9	0.708174
Y1-24	6223.9	0.204	0.39	0.042	0.157	0.033	0.007	0.033	0.003	0.028	0.006	0.018	0.003	0.017	0.003	0.944	0.064	0.583	16.26	2.002	1.67	−0.36	115.4	0.708197
Y1-1	6243.61	0.214	0.406	0.047	0.174	0.036	0.01	0.038	0.004	0.024	0.004	0.011	0.001	0.009	0.002	0.98	0.031	0.149	6.107	81.97	2.48	−1.58	65.27	0.707997
Finely to medium crystalline dolomites																								
P1-9	5812.2	0.131	0.224	0.028	0.101	0.019	0.006	0.018	0.002	0.016	0.004	0.009	0.002	0.009	BT	0.57	0.089	0.862	69.66	9.39	1.40	−7.17		
P1-8	5812.8	0.117	0.213	0.026	0.104	0.022	0.007	0.017	0.004	0.018	0.004	0.011	0.002	0.012	BT	0.558	0.028	0.827	15.41	31.99	1.40	−7.04		
P1-7	5813.55	0.055	0.093	0.012	0.039	0.011	0.006	0.01	0.002	0.013	0.003	0.006	0.001	0.006	BT	0.258	0.02	0.439	54.28	44.98	1.00	1.00		
P1-2	5826.55	0.158	0.297	0.036	0.154	0.028	0.012	0.029	0.007	0.029	0.005	0.015	0.002	0.015	0.002	0.789	0.053	1.45	27.75	117.3	2.14	−6.83		
Y1-30	6181.20	0.065	0.122	0.016	0.056	0.008	0.005	0.012	0.001	0.009	0.002	0.007	0.002	0.009	BT	0.31	0.034	0.416	9.333	16.06	1.66	−6.23	173.7	0.708213
Y1-25	6196.72	0.096	0.172	0.018	0.072	0.019	0.027	0.015	0.002	0.01	0.002	0.006	0.002	0.007	BT	0.45	0.012	0.496	8.637	26.8	2.37	−6.47	209.8	0.707961
Y1-19	6206.95	0.15	0.289	0.033	0.117	0.022	0.014	0.02	0.002	0.011	0.002	0.007	0.002	0.006	BT	0.68	0.049	0.269	6.194	68.2	2.71	−0.19	98.67	0.708139
Y1-8	6230.02	0.503	0.916	0.103	0.4	0.072	0.057	0.094	0.011	0.05	0.01	0.026	0.004	0.025	0.003	2.274	0.067	1.721	29.11	40.2	2.32	−7.72	182.9	0.707797
Y1-7	6231.10	0.233	0.433	0.051	0.186	0.032	0.01	0.03	0.004	0.024	0.004	0.013	0.002	0.011	0.002	1.034	0.043	0.572	11.78	15.14	2.48	−6.66	140.7	0.707907
Y1-6	6234.12	0.123	0.229	0.028	0.099	0.017	0.017	0.021	0.002	0.013	0.003	0.006	0.002	0.006	0.002	0.566	0.034	0.087	5.757	14.62	2.30	−7.45	109.8	0.707847
Y1-4	6236.70	0.226	0.423	0.049	0.179	0.035	0.017	0.034	0.005	0.026	0.005	0.015	0.002	0.015	0.002	1.033	0.056	0.978	16.47	62.77	2.42	−1.53	127	0.708174
Dolomitic grainstones																								
P1-12	5764.20	0.106	0.202	0.027	0.088	0.022	0.011	0.016	0.003	0.014	0.003	0.008	0.002	0.007	0.002	0.509	0.015	0.792	34.29	70.55	1.44	−6.05		
P1-11	5766.37	0.107	0.186	0.019	0.077	0.016	0.011	0.013	0.002	0.009	0.002	0.006	0.002	0.006	0.002	0.456	0.017	0.384	4.95	117.1	0.06	1.51		
P1-6	5819.1	0.141	0.231	0.025	0.101	0.019	0.02	0.015	0.003	0.016	0.003	0.009	0.002	0.008	0.002	0.594	0.023	5.153	4.962	27.1	1.81	−7.10		
P1-5	5821.8	0.257	0.466	0.054	0.199	0.044	0.019	0.043	0.007	0.036	0.007	0.02	0.003	0.017	0.002	1.174	0.098	2.2	47.6	20.1	2.26	−6.72		
Y1-40	6119.37	0.164	0.277	0.032	0.113	0.019	0.029	0.025	0.003	0.014	0.003	0.007	BT	0.007	BT	0.695	0.054	0.217	23.38	6.702	1.27	−6.34	127.6	0.708069
Y1-38	6122.56	0.129	0.237	0.025	0.095	0.017	0.006	0.028	0.004	0.01	0.002	0.004	BT	0.005	BT	0.564	0.095	0.536	9.844	12.3	1.53	−5.71	83.52	0.708119
Y1-35	6127.03	0.181	0.351	0.043	0.163	0.031	0.011	0.037	0.004	0.024	0.005	0.015	0.002	0.013	0.002	0.882	BT	BT	BT	BT	1.64	−5.54	229.8	0.707775
Y1-34	6168.08	0.126	0.228	0.028	0.092	0.017	0.011	0.041	0.002	0.013	0.004	0.008	0.001	0.01	BT	0.582	0.018	1.036	11.92	34.31	1.27	−5.9	220.7	0.708147
Y1-32	6174.23	0.058	0.097	0.013	0.038	0.007	0.011	0.005	0.002	0.006	0.002	0.004	0.002	0.004	BT	0.25	0.033	0.194	5.993	47.51	0.96	−6.7	214.1	0.707516
Y1-31	6177.22	0.077	0.139	0.017	0.054	0.013	0.006	0.011	0.001	0.009	0.003	0.008	0.001	0.007	BT	0.347	0.034	0.208	6.928	12.23	0.75	−7.21	221.2	0.707873
Y1-29	6184.85	0.109	0.21	0.027	0.093	0.02	0.009	0.022	0.004	0.016	0.004	0.01	0.002	0.011	0.002	0.54	0.082	0.343	7.287	19.59	1.95	−6.03	495.1	0.707678

Table 1. *Cont.*

Sample NO.	Depth (m)	La	Ce	Pr	Nd	Sm	Eu	Gd	Tb	Dy	Ho	Er	Tm	Yb	Lu	ΣREE	Th	Zr	Ti	Ba	$\delta^{13}C$	$\delta^{18}O$	Sr	$^{87}Sr/^{86}Sr$
Y1-13	6222.71	0.148	0.282	0.034	0.139	0.031	0.036	0.031	0.003	0.022	0.005	0.011	0.002	0.012	0.002	0.758	0.057	0.311	8.936	232.3	2.65	−3.46		
Y1-2	6242.50	0.109	0.22	0.029	0.105	0.012	0.005	0.017	0.003	0.015	0.003	0.009	0.001	0.007	BT	0.54	0.036	0.692	7.111	4.295	2.46	−1.51	375.2	0.707766
Dolomitic microbialites																								
P1-4	5823.48	0.167	0.224	0.024	0.091	0.016	0.003	0.016	0.002	0.01	0.002	0.005	0.002	0.005	BT	0.567	0.018	0.383	8.873	10.66	1.63	−3.26		
Y1-33	6171.23	0.184	0.338	0.038	0.115	0.024	0.006	0.025	0.002	0.011	0.002	0.004	0.002	0.006	BT	0.758	0.043	0.267	3.495	14.49	2.32	−4.98	121.9	0.708057
Y1-22	6200.51	0.16	0.256	0.03	0.107	0.015	0.011	0.019	0.002	0.013	0.003	0.009	0.002	0.007	BT	0.63	0.031	0.349	4.049	39.83	2.27	−5.19	81.95	0.707745
Y1-21	6201.70	0.208	0.369	0.038	0.14	0.026	0.027	0.032	0.006	0.022	0.006	0.014	0.004	0.014	0.004	0.91	0.059	0.753	15.2	137.8	2.28	−5.61	75.22	0.707648
Y1-20	6205.00	0.182	0.339	0.044	0.148	0.033	0.01	0.027	0.004	0.022	0.005	0.015	0.003	0.023	0.003	0.86	0.219	3.745	4.505	22.69	2.49	−5.27	123	0.708018
Y1-18	6208.83	0.308	0.629	0.073	0.275	0.046	0.031	0.054	0.008	0.041	0.007	0.023	0.004	0.02	0.002	1.52	0.076	1.359	37.11	128.8	0.90	−5.68	117.1	0.708219
Y1-17	6209.73	0.475	0.978	0.112	0.385	0.072	0.027	0.07	0.008	0.048	0.01	0.029	0.004	0.023	0.003	2.24	0.095	1.211	40.12	69.98	2.65	−3.29	75.54	0.707546
Y1-16	6214.99	0.406	0.88	0.113	0.44	0.093	0.028	0.092	0.011	0.067	0.014	0.036	0.005	0.038	0.005	2.23	0.126	3.392	88.82	54.28	2.59	−5.57	89.58	0.708283
Y1-15	6216.43	0.29	0.549	0.064	0.218	0.041	0.018	0.038	0.005	0.031	0.006	0.018	0.002	0.015	0.002	1.297	0.036	0.396	11.8	72.09	2.65	−3.92	89.72	0.708224
Y1-11	6224.40	0.314	0.665	0.083	0.296	0.07	0.022	0.086	0.009	0.054	0.011	0.029	0.005	0.03	0.005	1.679	0.108	0.851	36.5	117.1	2.20	−3.56	230.9	0.707675
Y1-10	6225.54	0.953	2.132	0.231	0.902	0.175	0.044	0.172	0.024	0.128	0.024	0.062	0.011	0.06	0.01	4.928	0.223	4.536	10.32	14.13	2.56	−4.54	118.7	0.707646
Y1-9	6228.14	0.632	1.204	0.131	0.493	0.096	0.041	0.093	0.013	0.073	0.014	0.036	0.005	0.034	0.005	2.87	0.133	2.2	62.48	128.3	2.35	−4.59	177.8	0.707906
Y1-5	6235.70	0.145	0.283	0.034	0.125	0.024	0.007	0.024	0.002	0.018	0.004	0.012	0.002	0.009	0.001	0.69	0.003	0.229	6.765	8.618	2.48	−4.55		
Limestones																								
Y1-37	6121.35	0.058	0.093	0.012	0.042	0.007	0.002	0.007	0.002	0.008	0.002	0.006	0.001	0.005	BT	0.245	0.103	0.334	7.393	1.772	2.29	−3.69	410.9	0.707735
Y1-39	6123.66	0.166	0.289	0.04	0.137	0.028	0.006	0.023	0.006	0.026	0.004	0.012	0.002	0.011	0.002	0.752	0.061	0.8	19.59	3.093	2.22	−2.30	340.5	0.707731
Y1-36	6124.95	0.124	0.253	0.024	0.107	0.023	0.006	0.022	0.004	0.02	0.004	0.011	0.002	0.011	0.002	0.613	0.038	0.274	9.797	23.92	1.77	−3.42		
Y1-27	6188.60	0.157	0.309	0.035	0.113	0.028	0.007	0.036	0.003	0.018	0.004	0.011	0.002	0.01	0.002	0.73	0.055	0.976	22.95	38.71	1.69	−3.37	183.4	0.708024

4. Results

4.1. Petrography

Petrographic, SEM, and core investigations allowed the identification of five main categories of carbonate precipitates in the Middle Triassic Leikoupo Formation marine carbonate. These categories are limestones, very finely to finely crystalline dolomites, finely to medium crystalline dolomites, dolomitic grainstones, and dolomitic microbialites (Figures 4–6).

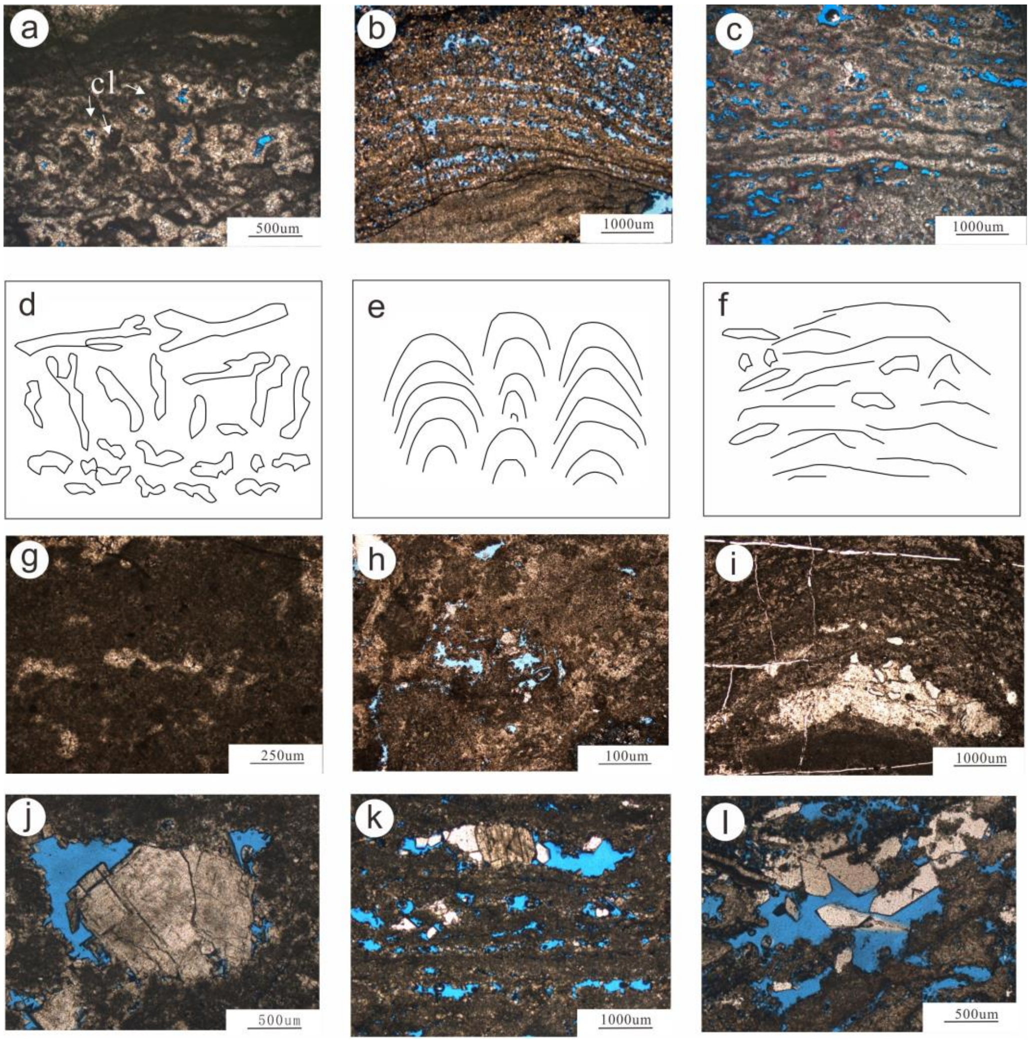

Figure 5. (**a**) Thin-section photomicrograph of dolomitic thrombolites with irregular vugs. Features labeled 'cl' (black and white) are mesoclots that comprise the clotted framework. The cavities are blue components filled with resin. Y1-9, 6228.14 m. (**b**) Thin-section photomicrograph of the stromatolitic laminae of alternating light and dark layers. Abundant cavities defined by deformed dark layers and roll-up structures. Y1-10, 6225.54 m. (**c**) Thin-section photomicrograph of thrombolitic stromatolites. Y1-22, 6200.51 m. (**d**) Sketch representing the pattern of the microbial texture in (**a**). (**e**) Sketch representing the pattern of the microbial texture in (**b**). (**f**) Sketch representing the pattern of the microbial texture in (**c**). (**g**,**h**) Peloid structures in the thrombolite. Y1-9, 6228.14 m. (**i**) Amalgamation of peloids in the mound structures in stromatolites. Y1-15, 6216.43 m. (**j**) Thin-section photomicrograph of saddle dolomite filling in pores in thrombolitic dolomites. Y1-33, 6171.23 m. (**k**) Quartz and dolomite filling in pores (dolomitized stromatolites). Y1-21, 6201.70 m. (**l**) Hexagonal dipyramidal high-temperature quartz filling in pores (dolomitized stromatolite). Y1-21, 6201.70 m.

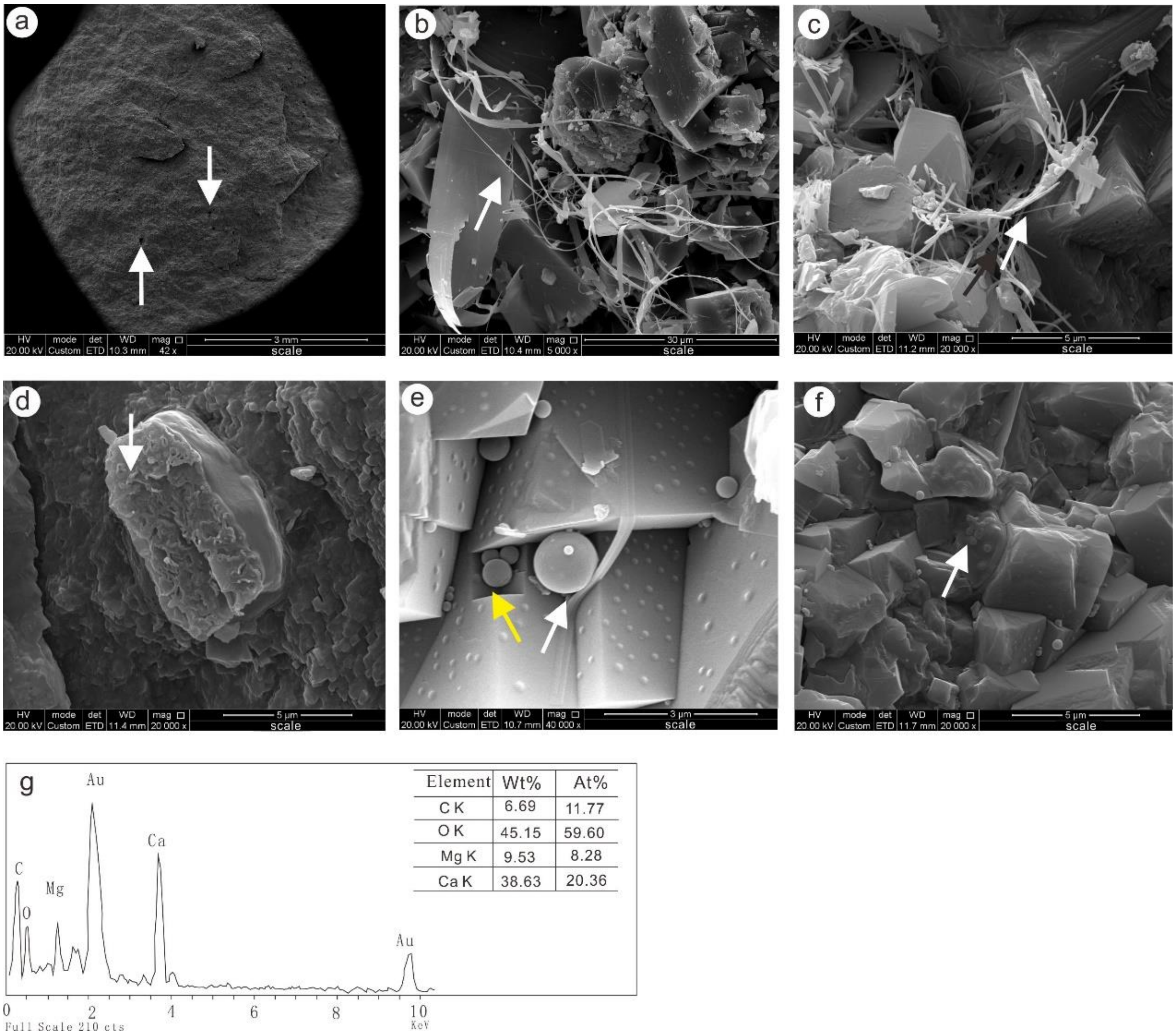

Figure 6. SEM photomicrographs and EDX analyses showing the characteristics of micron-sized structures in the Triassic microbialites. (**a**) Freshly broken fragment of thrombolitic dolomite, white arrows indicating the laminae studied under SEM. Y1-5, 6235.70 m. (**b**,**c**) Filament and sheet-like structures are well-preserved within the intercrystalline space. Subpolygonal and euhedral dolomite crystals connected by irregular filamentous and sheet-like textured materials (arrows) protruding from the spheroid matrix (arrows). Y1-5, 6235.70 m. (**d**) Spheroids (arrows) surrounded by an irregular lumpy texture, interpreted as mineralized degraded organic matter. Y1-20, 6205.00 m. (**e**) Spheroidal structures ranging in diameter from 100 nm to 1 µm are enclosed within dolomite crystals and protrude from them (arrows). Spherulitic dolomite occurring in a dolomite crystal defect (yellow arrows). Y1-20, 6205.00 m. (**f**) Chain of spheroids with individual spheroid diameters of 100–250 nm that protrude from the spheroid matrix (white arrows). The pyrite is well preserved within the irregular filamentous and sheet-like textured materials. Y1-20, 6205.00 m. (**g**) EDS spectrum showing a typical composition of the dolomite crystals in (**b**–**f**).

Limestone samples came from drill holes in the upper of Lei 4^3. The limestone samples are dark gray, and their lithology ranges from limy mudstone to finely crystalline dolomitic limestone less than 30 µm in size (Figure 5a). In a few cases, bioclasts such as foraminifera, brachiopoda, and shell fragments can be observed in the limestone samples. The limestone bed is commonly thin (usually 5 mm thick or less) and tight.

The very finely to finely crystalline dolomites (DOL-1) consist of subhedral to euhedral dolomite crystalline sized less than 30 µm (Figure 5b). In hand specimens, the very finely to finely crystalline dolomites are generally gray to dark gray in color. The DOL-1 samples from the bottom of Lei 4^3 are commonly associated with lamellar evaporitic anhydrite. Cryptocrystalline to crystalline pyrites are commonly dispersed within intercrystalline pores (Figure 5b). The DOL-1 dolomites have very low porosity and permeability values, with minor fractures filled with anhydrite. In places, dolomite crystals are truncated by stylolites. Volumetrically, this assemblage accounts for approximately 40% of the dolomite rocks in the basin via an approximate estimation based on well logging, cores, and thin sections.

The finely to medium crystalline dolomites (DOL-2) consist of anhedral to subhedral dolomite crystals, ranging in size from 30 µm to 150 µm (Figure 5c). In places, the DOL-2 dolomites replace precursor limestones (Figure 5d). The DOL-2 dolomites have relatively high porosity (average 5%) and permeability values due to abundant vugs and dissolution pores (Figure 5e). In a few cases, dissolution pores in a minority of samples of MD2 are also partly filled with late saddle dolomite, quartz, and/or fluorite. Volumetrically, MD2 dolomites make up approximately 20% of the dolomite rocks.

Dolomitic grainstones (DOL-3) primarily include oolitic dolomites and pelletal dolomitic grainstones (Figure 5f). The oolitic dolomites are usually gray and flaggy with an obvious oolitic structure and needle-shaped pores in the core. The ooids are present in the form of negative or hollow ooids that are partially or fully filled by fibrous and granulated calcite cement, with a cement content of usually 10–25%. The pelletal dolomitic grainstones are gray-light brown and contain a small number of bioclasts, such as brachiopods and foraminifera. In places, the space between grains is partly or totally filled with sparry calcite cement. Dolomitic grainstones have relatively high porosity (approximately 5–7%) and permeability values. Volumetrically, this type of dolomite constitutes approximately 15% of the rocks.

The dolomitic microbialites (MD) contain three types of microbial structures, which are discussed below (Figure 5): (a) Thrombolites (clotted, Figure 5a,d); (b) stromatolites (Figure 5b,e) and (c) thrombolitic stromatolites (Figure 5c,f). The microbialites in the western Sichuan Basin are commonly bedded, with bedding thicknesses ranging from tens of centimeters to meters. The thrombolites, thrombolitic stromatolites, and stromatolites are interbedded on a scale of centimeters to meters. Volumetrically, microbialites make up approximately 25% of the dolomite rocks. The detailed petrographic features of the microbialites are described as follows.

Thrombolites without lamination structures are composed of an irregularly clotted framework around structural cavities that are partly or totally filled with internal sediment and cement. Both clotted and cement textures consist of very finely to finely crystalline dolomites with crystalline sizes of less than 25 µm (Figure 5a). Framework components are generally dark because of the abundant organic inclusion in thin sections and constitute between 65 and 95% of the thrombolitic structure (Figure 5a,d). The sizes of those cavities are <1 mm normally, and large cavities are absent from densely clotted thrombolitic microbialites. The boundaries of cavities are defined by thrombolitic clots. Amalgamation or intergrowths of peloids 10–50 µm in size are clearly visible mesoscopically in some clots in the thrombolite buildup (Figure 5g,h). In a few cases, vugs in a minority of thrombolite samples are also partly filled with quartz and/or saddle dolomite (Figure 5j).

The stromatolitic dolomite is composed of microbial buildups of columnar and domal stromatolites with wavy laminations (Figure 5b,e). The main internal structures of the stromatolites are crinkly laminations. Crinkly laminations are wavy alternations of light and dark layers. The layers are generally isopachous, with light layers varying from 25 µm to 250 µm in thickness and dark layers varying from 25 µm to 500 µm in thickness. Both light and dark layers consist of very finely to finely crystalline dolomite crystals 5–60 µm in size. In general, light layers have abundant cavities defined by deformed dark layers and roll-up structures. The amalgamation of peloids is mesoscopically visible in some clots in the stromatolite buildup (Figure 5i). In a few cases, cavities in minority samples of stromatolites are also partly filled with quartz and/or fluorite (Figure 5k,l). The microbial dolimates that include stromatolites with thicknesses of 0.5–10 m have the highest porosity (average 7%) in the western Sichuan Basin.

The thrombolitic stromatolites (Figure 6c,f) are composite microbialites composed of clotted (thrombolites) and laminated (stromatolites) textures that intermingle on a subcentimeter scale. Microbial clots in the thrombolitic stromatolites are most commonly associated with discontinuous laminae and are densely packed along the irregular surfaces of voids. Stacks of millimeter-thick laminae alternate with layers of clots.

SEM photomicrographs of the dolomitic microbialite samples illustrate the nanometer-scale characteristics of dolomites (Figure 6a). Notably, various morphologies, such as filamentous (Figure 6b,c), sheet-like (Figure 6c), and rod-shaped (Figure 6b), are enclosed within the dolomite crystals (Figure 6d). Nanometer-sized spheroids, ranging in diameter from 100 nm to 1 μm, occur on the surface of the dolomite crystals or at dolomite crystal defects (Figure 6f). Adjacent dolomite crystals are connected by filaments to form a reticular pattern draping the crystals. According to energy-dispersive X-ray spectroscopy, these various poorly crystallized structures enclosed within the dolomite crystals show a typical composition of the dolomite crystals (Figure 6g).

4.2. Geochemistry

The trace element and isotope data for distinct carbonate categories are summarized in Table 1. The trace element and petrographic results are discussed separately for each category: (1) Limestones; (2) very finely to finely crystalline dolomites; (3) finely to medium crystalline dolomites; (4) dolomitic grainstones; and (5) dolomitic microbialites. The REEs in very finely or finely crystalline dolomites, as well as in limestones, which were not significantly influenced by later-stage diagenesis, can serve as proxies for the ancient seawater REE composition, thereby providing important information on the diagenetic history of these rocks through comparison with the REE signatures of the diagenetic carbonates [2,26].

Table 1 shows the REE contents, stable and radioactive isotope compositions, and trace element concentrations for carbonate samples in the western Sichuan Basin. All concentrations are in parts per million (ppm), except where noted. C and O isotope compositions are both reported relative to V-PDB. Moreover, the concentrations are below detection limits.

The various carbonate components yield important and consistent differences in the distributions of REEs despite very close proximity. The results show that the distribution coefficient of REEs between dolomite and seawater is high. However, the ΣREE value is still very low, and all of the data are less than 10 ppm (Table 1). The measured concentrations of Zr and Th are very low (Zr < 5.2 ppm, Th < 0.25 ppm, Ti < 90 ppm, Table 1). None of the total REE concentrations of the samples were correlated with Zr (R^2 = 0.35, Figure 7a) or Ti (R^2 = 0.13, Figure 7b). These results indicate that the REE compositions of the dolomite were not contaminated by impurities, such as clay minerals and fluvial clastic sediment.

The remaining 45 samples in the Leikoupo Formation have relatively consistent patterns overall (Table 1, Figure 8). These include (1) relatively low REE concentrations (mean ΣREE =1 ppm; standard deviation (SD) = 0.83 ppm; range: 0.21 to 4.93 ppm); (2) strong LREE enrichment [mean $(Nd/Yb)_{sn}$ = 4.34, SD = 1.17]; (3) notable positive Ce anomalies (mean $(Ce/Ce^*)_{sn}$ = 6.6, SD = 0.37) and negative Pr anomalies (mean $(Pr/Pr^*)_{sn}$ = 0.23, SD = 0.017; Figure 6); (4) mostly no Gd anomalies, with Gd anomalies of ≈ 1 (mean $(Gd/Gd^*)_{sn}$ = 1.03, SD = 0.3), ranging from 0.3 to 1.4; and (5) the Eu anomalies are mostly positive (mean $(Eu/Eu^*)_{sn}$ = 2, SD = 0.61), ranging from 0.82 to 7.8.

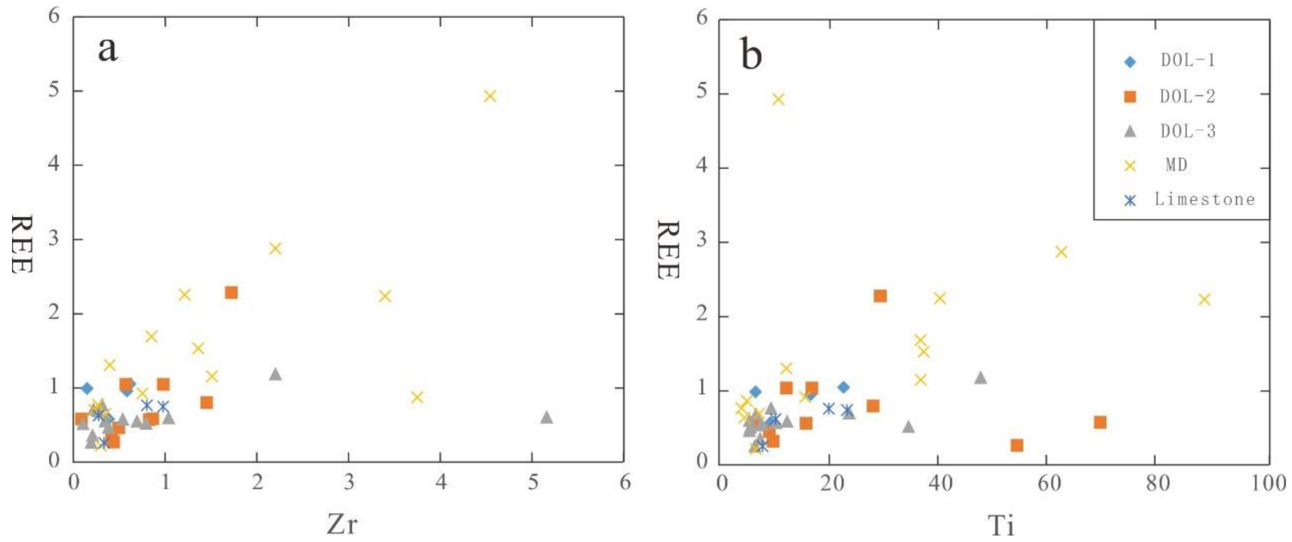

Figure 7. (**a**) Plot of Zr versus total REE concentration for dolomites and calcites in the Leikoupo Formation. (**b**) Plot of Ti versus total REE concentration for dolomites and calcites. Note that the total REE concentrations do not increase with the Zr or Ti content, suggesting that the total REE concentrations are not linked to extraneous terrigenous sediment.

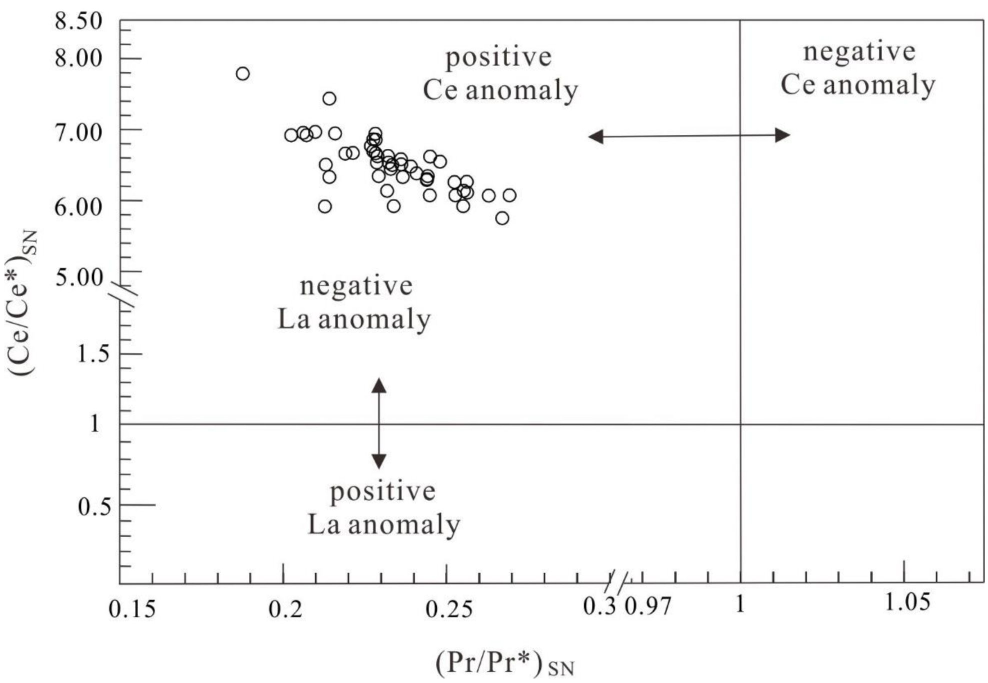

Figure 8. Plot of seawater-normalized Pr/Pr* [$2Pr_{SN}/(Ce_{SN} + Nd_{SN})$] versus Ce/Ce* [$2Ce_{SN}/(La_{SN} + Pr_{SN})$] (modified after Bau and Dulski (1996) [24]). Samples from the Leikoupo Formation. All samples show obvious positive Ce anomalies.

The limestone features mean ΣREE values of 0.59 ppm (SD = 0.23, Figure 9a), significant LREE enrichment (mean $(Nd/Yb)_{sn}$ = 3.6, SD = 0.61), positive Ce anomalies (mean $(Ce/Ce^*)_{sn}$ = 6.62, SD = 0.93), positive Eu anomalies ($(Eu/Eu^*)_{sn}$ = 1.11, SD = 0.12, ranging from 0.99 to 1.25), and no Gd anomalies $(Gd/Gd^*)_{sn}$ = 0.85, SD = 0.36, ranging from 0.61 to 1.37).

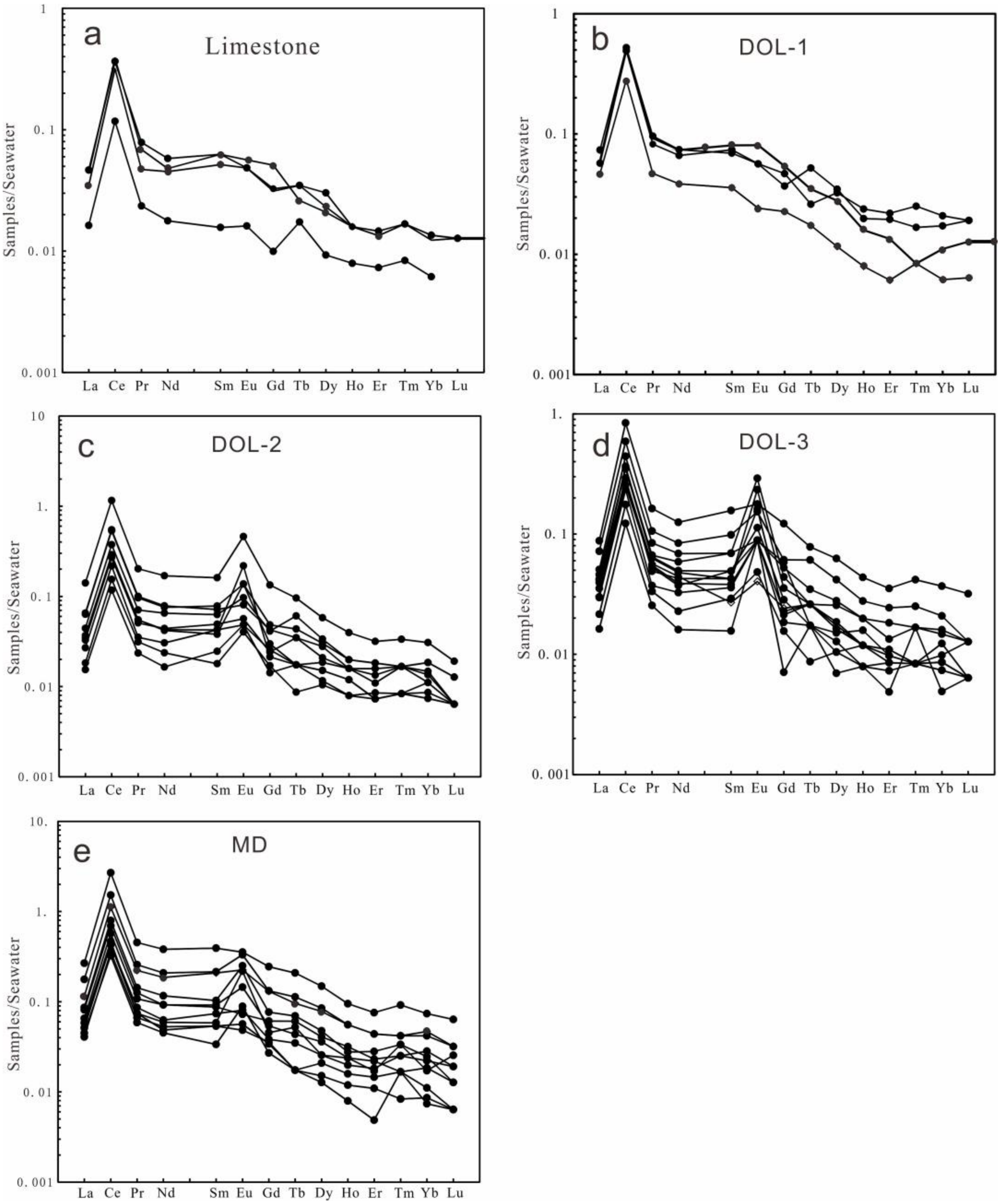

Figure 9. Seawater-normalized REE patterns of samples from the Leikoupo Formation. (**a**) Y1-73 is micritic dolomite, and the other three are all limy mudstone. (**b**) Very finely to finely crystalline dolomites (DOL-1). (**c**) Finely to medium crystalline dolomites(DOL-2). (**d**) Dolomitic grainstones(DOL-3). (**e**) Dolomitic microbialites(MD).

The very finely to finely crystalline dolomite (DOL-1) samples (n = 4) have relatively low REE concentrations (mean ΣREE = 0.88 ppm; SD = 0.21 range: 0.57 to 1 ppm, Figure 9b), significant LREE enrichment [mean $(Nd/Yb)_{sn}$ = 5.09, SD = 1.64], positive Ce anomalies (mean $(Ce/Ce^*)_{sn}$ = 6.5, SD = 0.48), and no Eu anomalies ($(Eu/Eu^*)_{sn}$ = 1.01, SD = 0.8, ranging from 0.82 to 1.19).

The finely to medium crystalline dolomites (DOL-2) have a mean ΣREE concentration of 0.78 ppm (SD = 0.58, n = 11, Figure 9c), significant LREE enrichment [mean $(Nd/Yb)_{sn}$ = 3.93, SD = 1.34], positive Ce anomalies (mean $(Ce/Ce^*)_{sn}$ = 6.49, SD = 0.29), and positive Eu anomalies ($(Eu/Eu^*)_{sn}$ = 2.72 SD = 1.65, ranging from 1.41 to 2.49).

The dolomitic grainstones (DOL-3) have a mean ΣREE concentration of 0.68 ppm (SD = 0.35, n = 14, Figure 9d), significant LREE enrichment (mean $(Nd/Yb)_{sn}$ = 4.31, SD = 1.22), positive Ce anomalies (mean $(Ce/Ce^*)_{sn}$ = 6.53, SD = 0.30), and positive Eu anomalies ($(Eu/Eu^*)_{sn}$ = 3.07, SD = 1.99, ranging from 1.24 to 7.8).

The dolomitic microbialites (MD) have higher REE concentrations than the DOl-1 dolomites (mean ΣREE = 1.67 ppm, SD = 1.25, ranging from 0.63 to 4.93, n = 15, Figure 9e) and feature significant LREE enrichment (mean $(Nd/Yb)_{sn}$ = 4.67, SD = 1.13), highly positive Ce anomalies (mean $(Ce/Ce^*)_{sn}$ = 6.77, SD = 0.35), and positive Eu anomalies ($(Eu/Eu^*)_{sn}$ = 1.89, SD = 0.96, ranging from 0.98 to 4.2).

The limestone samples have $\delta^{18}O$ values ranging from −2.3‰ to −3.7‰ and $\delta^{13}C$ values ranging from 1.7‰ to 2.3‰ (Figure 10). These carbon and oxygen stable isotope values fall within the field of the isotopic composition of Triassic seawater, with a range of 0.4‰ to 3.2‰ for $\delta^{13}C$ and −2.1‰ to −4.1‰ for $\delta^{18}O$ [13].

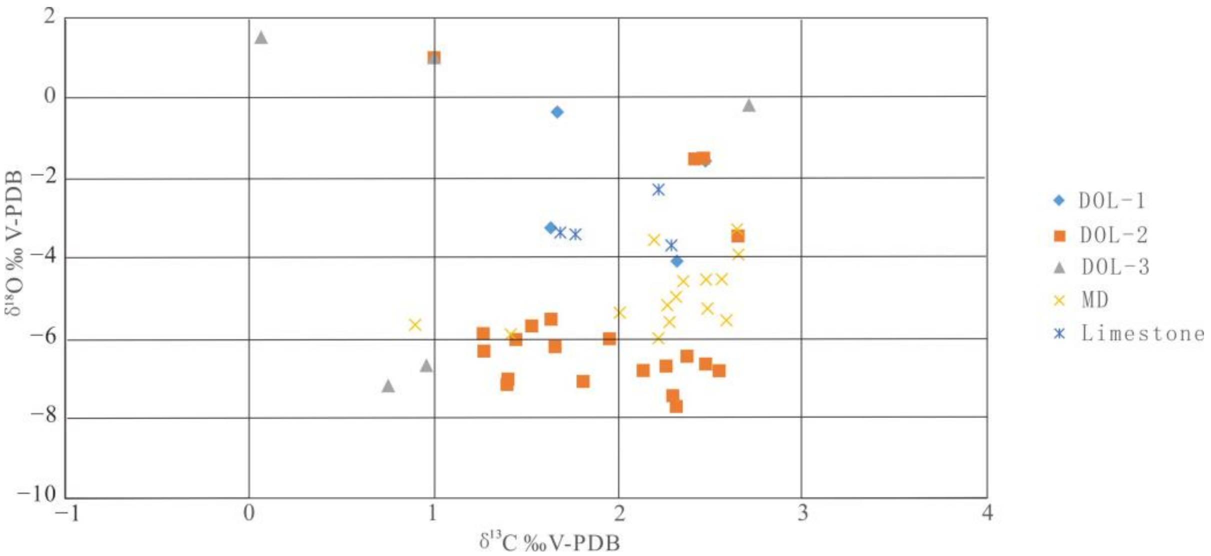

Figure 10. Plot of stable O and C isotope ratios for the carbonate from the Leikoupo Formation.

Thirty-four of the samples analyzed for oxygen and carbon isotopic compositions were also selected for Sr isotopic analysis (Table 1; Figure 10). The $^{87}Sr/^{86}Sr$ ratios are not correlated with Sr (R^2 = 0.14), and the weak negative correlation is caused by the isotope effect (Figure 11). The strontium isotopic compositions in the research area are not polluted by impurities, such as clay minerals or terrigenous clastic sediments. The $^{87}Sr/^{86}Sr$ ratios for the Leikoupo Formation limestone range from 0.707831 to 0.708309 (average 0.707968), close to the estimated $^{87}Sr/^{86}Sr$ ratio range (0.7083–0.70787) for Triassic seawater [27,28]. Only one sample has a value (0.00004) lower than the lower limit value (0.00006).

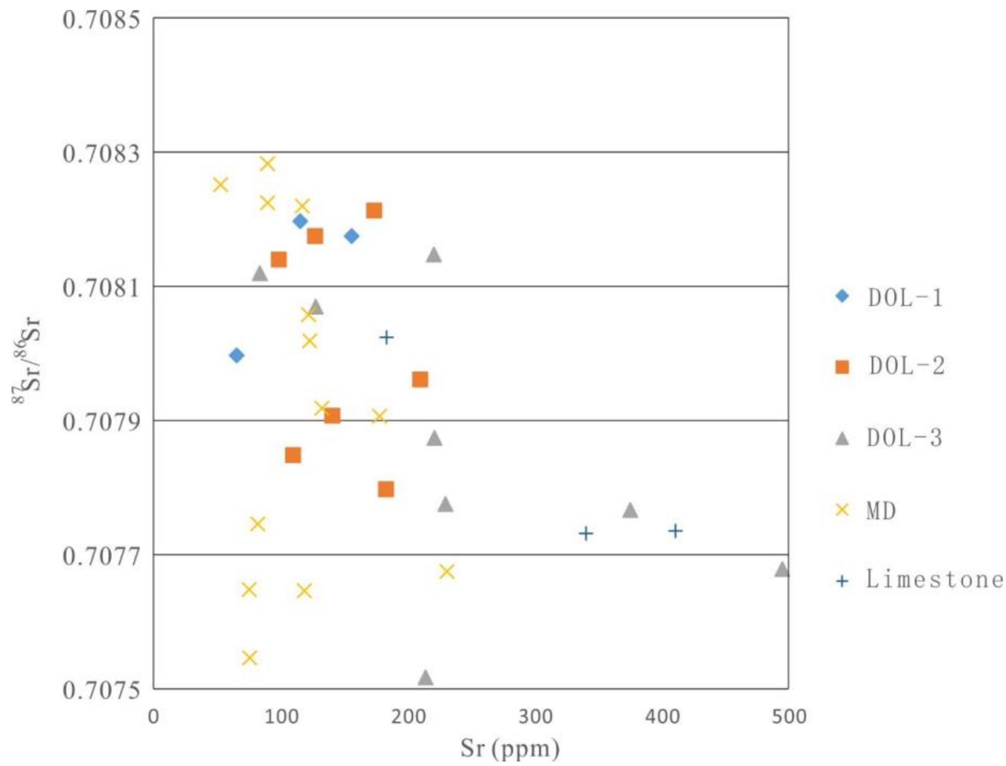

Figure 11. Plot of Sr isotope ratios versus Sr concentration for the carbonate from the Leikoupo Formation.

The $^{87}Sr/^{86}Sr$ ratios of the MD samples range from 0.707906 to 0.708225 (average 0.708023), completely falling within the range of the limestone samples (0.707831~0.708309).

5. Discussion

5.1. Average Surface Pacific Seawater as Normalized Standard and Ce Anomaly

The discussion of which materials are suitable for the normalization of geochemical samples is very important. Previous studies on REE geochemistry have usually utilized the standards Post-Archaean Australian Shale (PAAS), North American Shale Composite (NASC), and C1 chondrite [29,30]. Della Porta and Allwood [8,31] used the Mud standard to study microbial carbonate.

However, Limestone, the precursor of dolomite, inherits its REE distribution from seawater without the influence of terrestrial clastics [25]. Additionally, microbialites are organosedimentary deposits that accrete as a result of a benthic microbial community trapping and binding sediment and/or forming the locus of mineral precipitation [32], and many microbialites consist almost entirely of minerals precipitated directly from the ambient water [32,33]. Hence, the REEs in marine dolomites are primarily inherited from seawater and/or seawater-derived fluids. In addition, ancient microbialites commonly record the REE compositions of contemporary seawater [31], and the REE abundances are usually systematically different between particular average shales because of variations in the crustal rocks involved. Kawabe [34] found that PAAS shows a convex tetrad effect distribution when normalized by NASC. Therefore, choosing the REE concentration of standard seawater or equivalent marine limestone as the standard for normalization appears reasonable. Seawater has been suggested to be a suitable normalizing standard for REE studies of marine carbonates [29,35]. In this study, we discuss the REE characteristics of the Leikoupo Formation dolomite from this perspective.

The seawater-normalized REE patterns in most of our samples show obvious positive Ce anomalies (mean $(Ce/Ce^*)_{sn}$ = 6.6, SD = 0.37) (Figure 8). Ce anomalies, in particular negative anomalies, are widely believed to be a characteristic of seawater, regardless of whether the sample is normalized to PAAS or NASC [25,36]. This pattern occurs because oxidized Ce^{4+} is less soluble and more readily adsorbed onto particles than Ce^{3+}, and the extent of Ce depletion reflects the oxygenation state of the water [37,38]. Ce oxidation occurs preferentially at shallow water depths (e.g., Ref. [38]), and evidence of Ce oxidation in seawater has existed since the Paleoproterozoic [39]. Therefore, Ce is more enriched in marine carbonate than its REE neighbors lanthanum (La) and praseodymium (Pr) [39]. Thus, the seawater-normalized positive Ce anomaly is indicative of seawater.

5.2. Origins of DOL-1, DOL-2 and DOL-3

The carbon- and oxygen-stable isotope values of limestone samples falling within the isotopic field of Triassic seawater suggest that the geochemical characteristics of the limestones have not been modified by later diagenetic fluids. Hence, the limestone samples plausibly represent the Middle Triassic seawater. The DOL-1 dolomite samples have $\delta^{18}O$ values ranging from −0.4‰ to −4.1‰ and $\delta^{18}O$ values ranging from 1.7‰ to 2.5‰ (Figure 10). In addition, the DOL-1 samples have REE patterns (low REE concentrations, positive Ce anomalies, and positive La anomalies) similar to those of the marine limestone samples (Figure 8), suggesting that the REE patterns of the precursor limestones were not significantly altered during the formation of the very finely to finely crystalline dolomites. The DOL-1 dolomites are thus interpreted to represent penecontemporaneous dolomitization at or just below the sea floor by Middle Triassic seawater. Later diagenetic fluids did not significantly modify the REE patterns or other geochemical characteristics of these dolomites because of their low porosity and permeability. The lack of an obvious Eu anomaly is a common feature of the DOL-1 dolomites in the region, but most of the DOL-2, DOL-3, and MD dolomite samples show a positive Eu anomaly. Positive Eu anomalies have been identified in middle REE (MREE)-enriched early pore fluids [40] but may also reflect abundant weathering of plagioclase from a terrigenous or volcanic source [41]. In addition, Eu is enriched in highly reducing hydrothermal fluids [42,43], and many researchers have reported that Eu anomalies reflect a potential direct influence of hydrothermal fluids during burial [44,45]. As mentioned above, the REE compositions of the samples were not contaminated by impurities. The pore process of the Lei 4 dolomites in the Sichuan primarily Basin occurred parasyngenetically [46,47]. In addition, the samples with high porosity have more dissolution pores than the low-porosity DOL-1 samples, consistent with the influence of early pore fluids.

There are two taphrogenic events and related extensive fluid activities in the marine carbonate rocks in the Sichuan Basin, so hydrothermal dolomitization could be widespread [48]. Hydrothermal minerals are pervasive in the study area, which implies that there may be hydrothermal activity-related dolomite in the western Sichuan Basin [48]. According to systemic research on Sr isotopes, fluid inclusions, and lithology of the surrounding rocks and veins, Peng [49] reported that the Middle Triassic dolomite in the Sichuan Basin was influenced by hydrothermal activity. A late hydrothermal fluid influence is consistent with the presence of sparse saddle dolomite and idiomorphic quartz in our samples. However, this sparse saddle dolomite and idiomorphic quartz are disseminated in only four samples from the two cored wells. The influence of hydrothermal activity was not widespread, likely due to the tight very finely to finely crystalline dolomites and thick anhydrite in the Leikoupo Formation. Accordingly, we could not ignore the influence of early pore fluids.

5.3. Origins of Microbial Dolomites

The spherulitic dolomites feature structures similar to the spheroidal nanostructures of contemporaneous microbial dolomite described by Perri and Tucker [50]. SEM observations reveal the presence of spheroidal nanostructures, filaments, and sheet-like structures that are well preserved within the intercrystalline space in all microbialite samples. The nanometer-scale spherulitic dolomites occurring in the dolomite crystal defects suggest that poorly crystallized structures obstructed the growth of the dolomite crystals. This observation may imply that nanometer-scale spherulitic structures formed earlier than the dolomite crystals.

A thrombolite macrofabric is defined by the external shape of individual masses of microbial carbonate, such as clots or small shrub-like masses, and thrombolitic stromatolites, typified by some Shark Bay columns, are internally weakly clotted and crudely laminated [50,51]. The stromatolites, thrombolites, and thrombolitic stromatolites in the Leikoupo Formation formed in close temporal and spatial association, indicating that distinct microbialite forms developed in similar peritidal environments.

In addition, the $^{87}Sr/^{86}Sr$ ratios of the MD samples fall completely within the range of the limestone samples. Therefore, the dolomitizing fluids of the microbialites may have come from contemporaneous seawater.

The MD samples with significantly positive La and Eu anomalies have higher REE concentrations and $(Nd/Yb)_{sn}$ values (4.67 ± 1.13) than the limestones (mean $(Nd/Yb)_{sn}$ = 3.6, SD = 0.61), which is consistent with initial complexation on organic ligands in the biofilm. According to our previous discussion, the REE distribution of the limestones was preserved during the diagenesis process. Cooccurring carbonate components that presumably precipitated from the same seawater should have different relative REE concentrations but consistent REE patterns [41]. Differences in anomalies may provide some clues to help decipher the effects of formation fluids or microbial action on the evolution of the rock. Microbialite carbonates that record seawater-like REE signatures, that precipitated from seawater, and that have higher REE concentrations than synsedimentary cements are, in part, good proxies for seawater REE based on the observations of other studies on recent and ancient microbialites [7,8]. If the REE patterns of the limestones are taken to represent the Middle Triassic seawater, the data suggest that the microbialites were enriched in REEs and LREEs because bacterial photosynthesis and/or microbial respiration trapped and bound LREE-enriched organic colloids.

As documented above, the petrologic characteristics and isotopic analysis (C-O-Sr) suggest that the dolomitizing fluids of the microbialites were contemporaneous seawater.

Calibration of the $\delta^{18}O$ paleothermometer for dolomite precipitated in microbial cultures and natural environments [42] has provided a tool with which to calculate the temperature during early diagenetic dolomite precipitation and evaluate the conditions of ancient dolomite formation. The paleothermometers of the microbial dolomites in this study were calculated using the oxygen isotope fractionation factor of Vasconcelos et al. [42].

$$1000\ln\alpha_{dolomite-water} = 1000\times\ \ln\left(1000+\delta18\text{Odolomite}\right)/\left(1000+\delta18\text{Owater}\right)$$

$$= 2.73 \times 10^{6}\ T^{-2} + 0.26$$

The Triassic $\delta^{18}O$ values of calcites range from −4.1‰ to −2.1‰ PDB and are based on well-preserved low-magnesium calcite brachiopod shells from the Triassic [43]. The Triassic $\delta^{18}O$ values of well-preserved brachiopods from the Muschelkalk Formation range from −6.2‰ to −2‰ PDB [13]. Given the aridity and high temperatures of the Middle Triassic Sichuan Basin, plausible $\delta^{18}O$ values of coeval seawater from −4.2‰ to −2.1‰ SMOW were used in the calculation of dolomite paleotemperatures ($T_{seawater}$ = 20 °C) (Table 2).

Table 2. Oxygen isotopic values of dolomitic microbialites from the Middle Triassic in the western Sichuan Basin. The calculated paleotemperatures are for carbonate precipitation from Middle Triassic seawater.

Sample No.	Depth (m)	Lithology	$\delta^{18}O$ (‰)	$T^{max}_{dolomite}$ ($\delta^{18}O_{seawater}$ = −2.1‰) (°C)	$T^{min}_{dolomite}$ ($\delta^{18}O_{seawater}$ = −4.2‰) (°C)
P1-10	5808.30	The thrombolitic dolomite, the clotted consist of very finely crystalline dolomites with low porosity	−5.92	49.23	36.82
P1-3	5824.25	The thrombolitic dolomite, the clotted consist of very finely crystalline dolomites with low porosity	−6.02	49.85	37.37
Y1-33	6171.23	The thrombolitic dolomite, the clotted consist of very finely to finely crystalline dolomites crystalline sizes less than 25 μm	−4.98	43.59	31.79
Y1-23	6200.10	The stromatolitic dolomite	−5.38	45.95	33.90
Y1-22	6200.51	The stromatolitic dolomite	−5.19	44.82	32.89
Y1-21	6201.70	The very finely to finely crystalline dolomite of the stromatolite, crystals 5–60 μm in sizes.	−5.61	47.34	35.13
Y1-20	6205.00	The stromatolitic dolomite	−5.27	45.30	33.31
Y1-18	6208.83	The very finely to finely crystalline dolomite of the stromatolite, crystals 5–60 μm in sizes.	−5.68	47.76	35.51
Y1-17	6209.73	The dolomite of thrombolitic stromatolites	−3.29	34.15	23.34
Y1-16	6214.99	The thrombolitic dolomite, the clotted consist of very finely crystalline dolomites with low porosity	−5.57	47.09	34.91
Y1-15	6216.43	The stromatolitic dolomite	−3.92	37.57	26.40
Y1-11	6224.40	The thrombolitic dolomite, the clotted consist of very finely crystalline dolomites with low porosity	−3.56	35.60	24.64
Y1-10	6225.54	The dolomite of thrombolitic stromatolites	−4.54	41.04	29.52
Y1-9	6228.14	The thrombolitic dolomite, the clotted consist of very finely crystalline dolomites with low porosity	−4.59	41.33	29.77
Y1-5	6235.70	The thrombolitic dolomite, the clotted consist of finely crystalline dolomites crystals 25–60 μm in sizes	−4.55	41.10	29.57

The $T^{max}_{dolomite}$ and $T^{min}_{dolomite}$ values, listed in Table 2, range from 23.33 °C to 41.07 °C and from 34.15 °C to 49.85 °C, respectively. There are clear significant kinetic barriers to dolomite formation below approximately 50 °C [50]. Obviously, the paleotemperatures of the microbial dolomites in this study are less than 50 °C, and the $T^{max}_{dolomite}$ of two samples is lower than the temperatures at which dolomite precipitates in microbial cultures and natural environments [41]. The microfabric components are consistent with the mineral precipitate morphologies of dolomites in microbial mats. The nanospheroidal and irregular filamentous dolomites are very similar to those observed in culture experiments and in some modern dolomite-producing microbial mats with active bacterial communities, biofilms, and extracellular polymeric substances (EPS). Accordingly, microbial action was a significant factor in the dolomitization of the Leikoupo dolomitic microbialites, and evidence of microbial action is well preserved in the geological record. Based on the assumption of an annual average surface temperature of 20 °C and a normal geothermal gradient of 22–26 °C/km for the Middle Triassic to Lower Cretaceous successions [52,53], the formation of dolomitic microbialites in the Middle Triassic (Leikoupo Formation) was likely triggered by burial of these carbonates to depths between approximately 0 m and 800 m during the time interval from the early Middle Triassic to the Middle Triassic.

6. Conclusions

A wide variety of carbonate rocks were identified and described in the Middle Triassic Leikoupo Formation in the Sichuan Basin, including limestone, very finely to finely crystalline dolomites, finely to medium crystalline dolomites, dolomitic grainstones, and microbial dolomites. The different rocks that formed in different paleogeographic environments and diagenetic environments are characterized by different REE signatures. Therefore, REE analyses may provide useful information about the nature of dolomite and/or dolomitization processes.

The very finely to finely crystalline dolomites have REE patterns (low REE concentrations, positive Ce anomalies, and positive La anomalies) similar to those of the marine limestone samples. This similarity, in conjunction with oxygen and strontium isotopic signatures similar to those of Middle Triassic seawater, suggests that the dolomitizing fluid of dolomitic microbialites was Middle Triassic seawater and that later diagenetic fluids did not significantly modify these REE patterns.

In the Leikoupo Formation, the three types of dolomite (finely to medium crystalline dolomites, dolomitic grainstones, and dolomitic microbialites) with high porosity (i.e., the ones with more dissolution pores than the low-porosity very finely to finely crystalline dolomite) were influenced by early pore fluids and hydrothermal activity in the western Sichuan Basin.

The microbial action was a significant factor in the dolomitization of the dolomitic microbialites. Evidence of microbial action is well preserved in the Middle Triassic microbial dolomites in the Sichuan Basin.

Author Contributions: Conceptualization, H.W. and J.S.; methodology, H.W. and Z.Y.; validation, H.W., Z.Y. and J.S.; formal analysis, H.W.; investigation, H.W.; resources, T.L. and Y.Y.; data curation, H.W.; writing—original draft preparation, H.W.; writing—review and editing, Z.Y. and J.S.; supervision, Z.Y.; project administration, T.L. and Y.Y.; funding acquisition, Y.Y. and J.S. All authors have read and agreed to the published version of the manuscript.

Funding: This research was funded by the National Natural Science Foundation Key Program of China (Grant No. 41872150), and the Sichuan Science and Technology Program (Grant No. 2017JY0048).

Data Availability Statement: Not applicable.

Conflicts of Interest: The author declares no conflict of interest.

References

1. Guy, C.; Daux, V.; Schott, J. Behaviour of Rare Earth Elements During Seawater/Basalt Interactions in the Mururoa Massif. *Chem. Geol.* **1999**, *158*, 21–35. [CrossRef]
2. Qing, H.; Mountjoy, E.W. Rare earth element geochemistry of dolomites in the Middle Devonian Presqu'ile barrier, Western Canada Sedimentary Basin: Implications for fluid-rock ratios during dolomitization. *Sedimentology* **1994**, *41*, 787–804. [CrossRef]
3. Iannace, A.; Capuano, M.; Galluccio, L. "Dolomites and dolomites" in Mesozoic platform carbonates of the Southern Apennines: Geometric distribution, petrography and geochemistry. *Palaeogeogr. Palaeoclimatol. Palaeoecol.* **2011**, *310*, 324–339. [CrossRef]
4. Wang, G.; Li, P.; Hao, F.; Zou, H.; Zhang, L.; Yu, X. Impact of sedimentology, diagenesis, and solid bitumen on the development of a tight gas grainstone reservoir in the Feixianguan Formation, Jiannan area, China: Implications for gas exploration in tight carbonate reservoirs. *Mar. Pet. Geol.* **2015**, *64*, 250–265. [CrossRef]
5. Vasconcelos, C.; McKenzie, J.A.; Bernasconi, S.; Grujic, D.; Tiens, A.J. Microbial mediation as a possible mechanism for natural dolomite formation at low temperatures. *Nature* **1995**, *377*, 220–222. [CrossRef]
6. Warthmann, R.; van Lith, Y.; Vasconcelos, C.; McKenzie, J.A.; Karpoff, A.M. Bacterially induced dolomite precipitation in anoxic culture experiments. *Geology* **2000**, *28*, 1091–1094. [CrossRef]

7. Olivier, N.; Boyet, M. Rare earth and trace elements of microbialites in Upper Jurassic coral- and sponge-microbialite reefs. *Chem. Geol.* **2006**, *230*, 105–123. [CrossRef]
8. Della, P.; Webb, G.E.; McDonald, I. REE patterns of microbial carbonate and cements from Sinemurian (Lower Jurassic) siliceous sponge mounds (Djebel Bou Dahar, High Atlas, Morocco). *Chem. Geol.* **2015**, *400*, 65–86. [CrossRef]
9. You, X.; Sun, S.; Zhu, J.; Li, Q.; Hu, W.; Dong, H. Microbially mediated dolomite in Cambrian stromatolites from the Tarim Basin, north-west China: Implications for the role of organic substrate on dolomite precipitation. *Terra Nova* **2013**, *25*, 387–395. [CrossRef]
10. Guido, A.; Mastandrea, A.; Tosti, F.; Russo, F. Importance of rare earth element patterns in discriminating between biotic and abiotic mineralization. In *Advances in Stromatolite Geobiology*; Springer: Berlin/Heidelberg, Germany, 2011; pp. 453–462.
11. Corkeron, M.; Webb, G.E.; Moulds, J.; Grey, K. Discriminating stromatolite formation modes using rare earth element geochemistry: Trapping and binding versus in situ precipitation of stromatolites from the Neoproterozoic Bitter Springs Formation, Northern Territory, Australia. *Precambrian Res.* **2012**, *212*, 194–206. [CrossRef]
12. Warren, J. Dolomite: Occurrence, evolution and economically important associations. *Earth-Sci. Rev.* **2000**, *52*, 1–81. [CrossRef]
13. Korte, C.; Kozur, H.W.; Veizer, J. δ^{13}C and δ^{18}O values of Triassic brachiopods and carbonate rocks as proxies for coeval seawater and palaeotemperature. *Palaeogeogr. Palaeoclimatol. Palaeoecol.* **2005**, *226*, 287–306. [CrossRef]
14. Azmy, K.; Lavoie, D.; Wang, Z.; Brand, U.; Al-Aasm, I.; Jackson, S.; Girard, I. Magnesium-isotope and REE compositions of Lower Ordovician carbonates from eastern Laurentia: Implications for the origin of dolomites and limestones. *Chem. Geol.* **2013**, *356*, 64–75. [CrossRef]
15. Guo, C.; Chen, D.; Qing, H.; Zhou, X.; Ding, Y. Early dolomitization and recrystallization of the Lower-Middle Ordovician carbonates in western Tarim Basin (NW China). *Mar. Pet. Geol.* **2020**, *111*, 332–349. [CrossRef]
16. Xiong, L.L.; Suyan, W.X. Difference in depositional characteristics between intra-platform and marginal-platform shoals in Leikoupo Formation, Sichuan Basin and its impact on reservoirs. *Acta Pet. Sin.* **2011**, *32*, 70–75, (In Chinese with English abstract).
17. Bian, C.; Wang, Z.C.; Jiang, Q.; Chi, Y.; Xu, Z. Characteristics and distribution of karst reservoirs of Leikoupo Formation in western Sichuan Basin. *China Pet. Explor.* **2019**, *24*, 82–94.
18. Song, X.; Wang, Q.; Long, K. Characteristics and main controlling factors of Middle Triassic Leikoupo paleokarst reservoirs in western Sichuan Basin. *Mar. Orig. Pet. Geol.* **2013**, *18*, 8–14, (In Chinese with English abstract).
19. Wang, X.; Xin, Y.; Tian, H.; Zhu, M.; Zhang, H.; Li, W. Research progress on sedimentary reservoir of Leikoupo Formation in the Middle Triassic of Sichuan Basin. *Mar. Orig. Pet. Geol.* **2020**, *25*, 210–222.
20. Li, J.X.; Jiang, H.F. *Global Palaeo-Plate Reconstruction and Lithofacies Palaeogeography Atlas*; Geological Publishing House: Beijing, China, 2013; pp. 38–39. (In Chinese)
21. Liu, S.G.; Song, J.M.; Luo, P.; Qing, H.R.; Lin, T.; Sun, W.; Li, Z.W.; Wang, H.; Peng, H.L.; Yu, Y.Q.; et al. Characteristics of microbial carbonate reservoir and its hydrocarbon exploring outlook in the sichuan basin, China. *J. Chengdu Univ. Technol.* **2016**, *43*, 129–152, (In Chinese with English abstract).
22. Johnson, D.M.; Hooper, P.R.; Conrey, R.M. XRF analysis of rocks and minerals for major and Trace Elements on a Single Low Dilution Li-tetraborate Fused Bead. *Adv. X-ray Anal.* **1999**, *41*, 843–867.
23. Wu, G.; Xu, B.; Zhang, C.; Gao, S.; Yao, T. Geochemistry of dust aerosol over the Eastern Pamirs. *Geochim. Cosmochim. Acta* **2009**, *73*, 977–989. [CrossRef]
24. Bau, M.; Dulski, P. Distribution of yttrium and rare-earth elements in the Penge and Kuruman iron-formations, Transvaal Supergroup, South Africa. *Precambrian Res.* **1996**, *79*, 37–55. [CrossRef]
25. Webb, G.E.; Nothdurft, L.D.; Kamber, B.S.; Kloprogge, J.; Zhao, J.X. Rare earth element geochemistry of scleractinian coral skeleton during meteoric diagenesis: A sequence through neomorphism of aragonite to calcite. *Sedimentology* **2009**, *56*, 1433–1463. [CrossRef]
26. Bau, M.; Alexander, B. Preservation of primary REE patterns without Ce anomaly during dolomitization of Mid-Paleoproterozoic limestone and the potential re-establishment of marine anoxia immediately after the "Great Oxidation Event". *S. Afr. J. Geol.* **2006**, *109*, 81–86. [CrossRef]
27. Veizer, J.; Buhl, D.; Diener, A.; Ebneth, S.; Podlaha, O.G.; Bruckschen, P.; Jasper, T.; Korte, C.; Schaaf, M.; Ala, D.; et al. Strontium isotope stratigraphy: Potential resolution and event correlation. *Palaeogeogr. Palaeoclimatol. Palaeoecol.* **1997**, *132*, 65–77. [CrossRef]
28. Hu, Z.W.; Huang, S.J.; Qing, H.R.; Wang, Q.D.; Wang, C.M.; Gao, X.Y. Evolution and global correlation for strontium isotopic composition of marine triassic from huaying mountains, eastern sichuan, China. *Sci. China* **2008**, *51*, 540–549. (In Chinese) [CrossRef]
29. Tanaka, K.; Miura, N.; Asahara, Y.; Kawabe, I. Rare earth element and strontium isotopic study of seamount-type limestones in Mesozoic accretionary complex of Southern Chichibu Terrane, central Japan: Implication for incorporation process of seawater REE into limestones. *Geochem. J.* **2003**, *37*, 163–180. [CrossRef]
30. Leybourne, M.I.; Johannesson, K.H. Rare earth elements (REE) and yttrium in stream waters, stream sediments, and FeeMn oxyhydroxides: Fractionation, speciation, and controls over REE+Y patterns in the surface environment. *Geochim. Cosmochim. Acta* **2008**, *72*, 5962–5983. [CrossRef]
31. Allwood, A.C.; Kamber, B.S.; Walter, M.R.; Burch, I.W.; Kanik, I. Trace elements record depositional history of an Early Archean stromatolitic carbonate platform. *Chem. Geol.* **2010**, *270*, 148–163. [CrossRef]

32. Burne, R.V.; Moore, L.S. Microbialites: Organosedimentary deposits of benthic microbial communities. *Palaios* **1987**, 241–254. [CrossRef]
33. Riding, R. Microbial carbonates: The geological record of calcified bacterialalgal mats and biofilms. *Sedimentology* **2000**, *47* (Suppl. S1), 179–214. [CrossRef]
34. Kawabe, I. Convex tetrad effect variations in REE abundances of "North American shale composite" and "Post-Archean Australian average shale". *Geochem. J.* **1996**, *30*, 149–153. [CrossRef]
35. Wang, L.; Hu, W.; Wang, X.; Cao, J.; Chen, Q. Seawater normalized REE patterns of dolomites in Geshan and Panlongdong sections, China: Implications for tracing dolomitization and diagenetic fluids. *Mar. Pet. Geol.* **2014**, *56*, 63–73. [CrossRef]
36. Azmy, K.; Brand, U.; Sylvester, P.; Gleeson, S.A.; Logan ABitner, M.A. Biogenic and abiogenic low-Mg calcite (bLMC and aLMC): Evaluation of seawater-REE composition, water masses and carbonate diagenesis. *Chem. Geol.* **2011**, *280*, 180–190. [CrossRef]
37. Alibo, D.S.; Nozaki, Y. Rare earth elements in seawater: Particle association, shale-normalization, and Ce oxidation. *Geochim. Cosmochim. Acta* **1999**, *63*, 363–372. [CrossRef]
38. Frimmel, H.E. Trace element distribution in Neoproterozoic carbonates as palaeoenvironmental indicator. *Chem. Geol.* **2009**, *258*, 338–353. [CrossRef]
39. Nothdurft, L.D.; Webb, G.E.; Kamber, B.S. Rare earth element geochemistry of Late Devonian reefal carbonates, Canning Basin, Western Australia: Confirmation of a seawater REE proxy in ancient limestones. *Geochim. Cosmochim. Acta* **2004**, *68*, 263–283. [CrossRef]
40. Cabioch, G.; Camoin, G.F.; Webb, G.E.; Le Cornec, F.; Molina, M.G.; Pierre, C.; Joachimski, M.M. Contribution of microbialites to the development of coral reefs during the last deglacial period: Case study from Vanuatu (South-West Pacific). *Sediment. Geol.* **2006**, *185*, 297–318. [CrossRef]
41. Haley, B.A.; Klinkhammer, G.P.; McManus, J. Rare earth elements in pore waters of marine sediments. *Geochim. Cosmochim. Acta* **2004**, *68*, 1265–1279. [CrossRef]
42. Vasconcelos, C.; McKenzie, J.A.; Warthmann, R.; Bernasconi, S. Calibration of the $\delta^{18}O$ paleo-thermometer with dolomite formed in microbial cultures and natural environments. *Geology* **2005**, *33*, 317–320. [CrossRef]
43. Olivarez, A.M.; Owen, R.M. REE/Fe variations in hydrothermal sediments: Implications for the REE content of seawater. *Geochim. Cosmochim. Acta* **1989**, *53*, 757–762. [CrossRef]
44. Veizer, J.; Ala, D.; Azmy, K.; Bruckschen, P.; Buhl, D.; Bruhn, F.; Carden, G.A.; Diener, A.; Ebneth, S.; Godderis, Y.; et al. $^{87}Sr/^{86}Sr$, $\delta^{13}C$ and $\delta^{18}O$ evolution of Phanerozoic seawater. *Chem. Geol.* **1999**, *161*, 59–88. [CrossRef]
45. Machel, H.G. Early lithification, dolomitization, and anhydritization of Upper Devonian Nisku buildups, subsurface of Alberta, Canada. In *Reef Diagenesis*; Springer: Berlin/Heidelberg, Germany, 1986; pp. 336–356.
46. Parsapoor, A.; Khalili, M.; Mackizadeh, M. The behaviour of trace and rare earth elements (REE) during hydrothermal alteration in the Rangan area (Central Iran). *J. Asian Earth Sci.* **2009**, *34*, 123–134. [CrossRef]
47. Sheng, A.J.; Zhou, J.G. Origin of Triassic Leikoupo Dolostone Reservoirs in Sichuan Basin. *Mar. Orig. Pet. Geol.* **2008**, *13*, 19–27, (In Chinese with English abstract).
48. Liu, S.G.; Huang, W.M.; Zhang, C.J.; Zhao, X.F.; Dai, S.L.; Zhang, Z.J.; Qin, C. Research status of dolomite genesis and its problems in Sichuan Basin. *Lithol. Reserv.* **2008**, *2*, 6–15, (In Chinese with English abstract).
49. Peng, J. Study on the Middle Triassic Reservoir Rocks in the Front Area of Northern-Central Longmenshan Mountains and Its Adjacent Areas. Master's Thesis, Chengdu University of Technology, Chengdu, China, 2009; pp. 49–66, (In Chinese with English abstract).
50. Perri, E.; Tucker, M. Bacterial fossils and microbial dolomite in triassic stromatolites. *Geology* **2007**, *35*, 207–210. [CrossRef]
51. Riding, R. The nature of stromatolites: 3500 million years of history and a century of research. In *Advances in Stromatolite Geobiology*; Springer: Berlin/Heidelberg, Germany, 2011; pp. 29–74.
52. Wang, W.; Zhou, Z.; Guo, T.; Xu, C. Early Cretaceous-Paleocene geothermal gradients and Cenozoic tectono-thermal history of Sichuan Basin. Journal of Tongji University. *Nat. Sci.* **2011**, *39*, 606–613, (In Chinese with English abstract).
53. Xu, M.; Zhu, C.; Tian, Y.; Rao, S.; Hu, S. Borehole temperature logging and characteristics of subsurface temperature in the Sichuan Basin. *Chin. J. Geophys.* **2011**, *54*, 224–233, (In Chinese with English abstract). [CrossRef]

Disclaimer/Publisher's Note: The statements, opinions and data contained in all publications are solely those of the individual author(s) and contributor(s) and not of MDPI and/or the editor(s). MDPI and/or the editor(s) disclaim responsibility for any injury to people or property resulting from any ideas, methods, instructions or products referred to in the content.